High-Resolution MRI at 7 T of Local Strains in the Intervertebral Disc

A. C. Wright[1], J. Yoder[2], N. Tustison[3], J. Gee[3], F. W. Wehrli[1], and D. M. Elliott[2]
[1]Laboratory for Structural NMR Imaging, Department of Radiology, University of Pennsylvania, Philadelphia, PA, United States, [2]McKay Orthopaedic Research Laboratory, Department of Orthopaedic Surgery, University of Pennsylvania, Philadelphia, PA, United States, [3]Penn Image Computing and Science Laboratory, Department of Radiology, University of Pennsylvania, Philadelphia, PA, United States

Introduction
Degeneration and failure of the intervertebral disc (IVD) causes the majority of spine dysfunction (1). While its sole function appears to be purely mechanical, the ability to predict the mechanical behavior of the IVD is critical for understanding the contribution of mechanical loading to the degenerative process and in efforts to restore mechanical integrity to the degenerated disc through surgical procedures, implanted devices, tissue engineering and gene therapy. Structural models of musculoskeletal tissues to calculate internal stresses and strains are an essential technology to investigate mechanisms of injuries and failure. Moreover accurate models provide understanding to predict the consequence of surgical interventions, device implantation, and tissue engineering. The objective of this work therefore is to develop an image-based model of the IVD that incorporates the tissue's inhomogeneous, anisotropic, and nonlinear material properties, and we present initial results from strain mapping methods with axial and sagittal slices in the IVD.

Methods
Specimen preparation: Intact fresh frozen bovine tail was sectioned into a bone-disc-bone motion segment with musculature intact. The motion segment initially was imaged in a non-loaded state. The motion segment then was loaded in 1% phosphate buffered saline and allowed to creep for 8 hrs under 222.4 N (50 lbs). The motion segment then was embedded in paraffin wax to minimize creep relaxation and to maintain hydration during acquisition of the deformed image, using identical pulse sequence parameters.
MR image acquisition: To achieve high SNR, a custom-made RF coil was used that had been designed for imaging the ankle (2). Since there is no transmit body coil, a shielded Helmholtz pair local transmit coil with a decoupled 4-element phased array receive coil was used, interfaced to a Siemens 7 T whole-body MRI scanner. After gradient echo localizers were acquired in three orthogonal planes, a single-slice 2D turbo spin echo (TSE) sequence was run to acquire axial and sagittal images through the center of the IVD. The TSE parameters were as follows: TR/TE = 3000/14 ms, ETL = 7, BW = 130 Hz/pixel, FOV = 6 cm^2, matrix = 256x256, slice thickness = 2 mm, scan time ~ 2 min.
Strain map processing: The axial images before and after applied load were processed using an Advanced Normalization Tools (ANTS) algorithm (3). Upon MRI acquisition of the reference and loaded configurations, internal deformations were calculated employing the ANTS software library which replaces the previous methodology for determining 2D disc strain as described above. Application of ANTS offers important new benefits. First, in addition to the texture-based measures used in prior work to establish correspondences between material points in the different disc configurations, ANTS contains additional volume-specific similarity metrics which can be evaluated in the extension to analysis of 3D MRI data. Specifically, cross-correlation and mutual information measures can be assessed. Furthermore, the diffeomorphic transformation models in ANTS, due to intrinsic topological properties, are guaranteed to implement the continuum assumption and therefore produce physically plausible kinematic quantities.

Results
The images of the IVD were of excellent quality and showed fine details of the annulus fibrosus lamellae (Fig. 1). The strain values found in the sagittal plane for radial (E_{xx}) strain were 0.0041 ± 0.094, 0.24, -0.18, axial (E_{yy}) strain was 0.0018 ± 0.045, 0.037, -0.28, and shear (E_{xy}) strain -0.10 ± 0.068, 0.13, -0.11 (average, max, min respectively). Strain in the axial plane for radial (E_{xx}) were 0.052 ± 0.12, 0.52, -0.21, axial (E_{yy}) strain was 0.033 ± 0.099, 0.39, -0.17, and shear (E_{xy}) strain -0.015 ± 0.067, 0.20, -0.27 (average, max, min respectively).

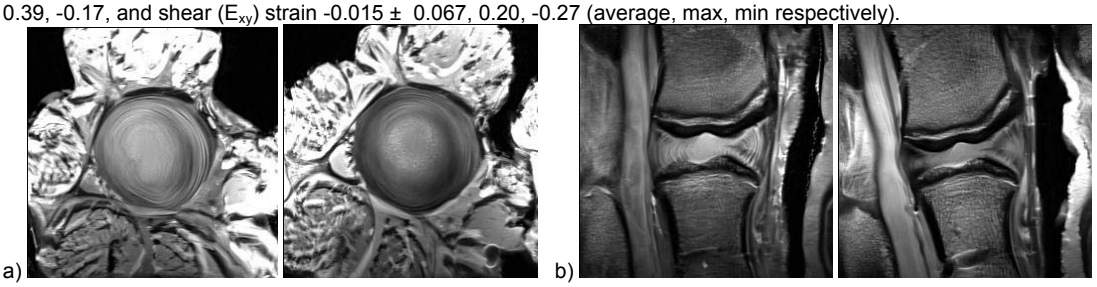

Fig. 1 Axial (a) and sagittal (b) images of the IVD before (left) and after (right) applied pressure using a 8-hr static load of 50 lbs. voxel = 230x230x2000 μm^3.

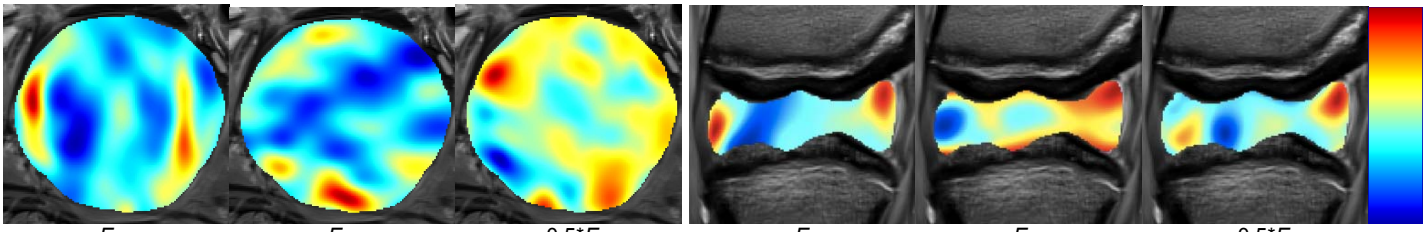

Fig. 2 Axial and sagittal strain maps in the IVD produced using ANTS algorithm. (blue = minimum, red = maximum strain).

Discussion
In this study strain has been analyzed in the axial plane of the disc non-invasively. The work was motivated by a study in which the internal disc strains were quantified from 2D MRI using a texture correlation mapping (4), and we observed similar strain trends. The internal disc deformations, including their contribution to interactions between the nucleus pulposus (NP) and annulus fibrosus (AF), were evaluated. In the sagittal plane we observed high tensile radial strains (E_{xx}) occurred in the posterior and anterior regions due to radial bulging. This was further demonstrated by radial strain in the axial plane showing high tensile strain in the outer AF. The axial strain (E_{yy}) displayed high tensile strains near the endplate due to the pressurization of the NP. Shear strains (E_{xy}) were non-uniform due to the uneven curvature of the bovine motion segment endplate. While some previous studies measured internal disc mechanics, these have been limited by the insertion of markers or other structural disruptions. In our studies the entire disc remains unaltered and intact. Based on the bovine tail disc area (5), the 222.4 N load represents 0.26 MPa stress which corresponds to approximately one half human bodyweight (5), and can therefore be considered physiologically relevant.

Acknowledgements: This work was supported by NIH grants RC1 AR058450, R01 AR053156, and P30 AR050950.
References: 1. asdfsd, et al., *Spine* **31**, 2151-61 (2006). 2. AC Wright, et al., *Proc. ISMRM 17th Meeting*, Honolulu, p. 2996 (2009). 3. B Avants, et al., ANTS: Advances open-source normalization tools for neuroanatomy. Penn Image Computing and Science Laboratory. 2009. 4. GD O'Connell, et al., *Spine* **32**, 2860-8 (2007). 5. JC Beckstein, et al., *Spine* **33**, E166–E173 (2008).